N O T I C E

THIS DOCUMENT HAS BEEN REPRODUCED FROM MICROFICHE. ALTHOUGH IT IS RECOGNIZED THAT CERTAIN PORTIONS ARE ILLEGIBLE, IT IS BEING RELEASED IN THE INTEREST OF MAKING AVAILABLE AS MUCH INFORMATION AS POSSIBLE

NASA

Technical Memorandum 82174

A MULTILAYER MODEL OF TIME DEPENDENT DEFORMATION FOLLOWING AN EARTHQUAKE ON A STRIKE-SLIP FAULT

Steven C. Cohen

AUGUST 1981

A MULTILAYER MODEL OF TIME DEPENDENT

DEFORMATION FOLLOWING AN EARTHQUAKE ON A

STRIKE-SLIP FAULT

Steven C. Cohen

Geodynamics Branch

Goddarc Space Flight Center

Greenbelt, Maryland 20771

August 1981

GODDARD SPACE FLIGHT CENTER
Greenbelt, Maryland

A MULTILAYER MODEL OF TIME DEPENDENT DEFORMATION FOLLOWING AN EARTHQUAKE ON A STRIKE-SLIP FAULT

Steven C. Cohen

Geodynamics Branch

Goddard Space Flight Center

Greenbelt, Maryland 20771

ABSTRACT

A multilayer model of the earth is used in finite element calculations of time dependent deformation and stress following an earthquake on a strike-slip fault. The model involves shear properties of an elastic upper lithosphere, a standard viscoelastic linear solid lower lithosphere, a Maxwell viscoelastic asthenosphere and an elastic mesosphere. Elastic dilatational properties are assumed throughout. Time dependent displacements, strains, and stresses are computed both at the surface of the earth and at depth. The analysis includes both systematic variations of fault and layer depths and comparisons with simpler elastic lithosphere over viscoelastic asthenosphere calculations. For conditions which may be appropriate for the earth both the creep of the lower lithosphere and asthenosphere can contribute to the postseismic deformation. The magnitude of the deformation is enhanced by a short distance between the bottom of the fault (slip zone) and the top of the creep layer but is less sensitive to the thickness of the creeping layer. Furthermore postseismic restressing is increased as the lower lithosphere becomes more viscoelastic, but the tendency for the width of the restressed zone to grow with time is retarded.

A MULTILAYER MODEL OF TIME DEPENDENT
DEFORMATION FOLLOWING AN EARTHQUAKE ON A
STRIKE-SLIP FAULT

INTRODUCTION

There is a growing body of evidence that postseismic ground deformation can be of geodetic

and tectonic significance following a major earthquake. In a number of cases there have been

direct observations of postseismic vertical and/or horizontal deformations (e.g. Thatcher, 1975;

Brown, et al., 1977; Thatcher, et al., 1980, Dunbar, et al., 1980). There are, in fact, a number

of mechanisms that have the potential to create significant postseismic deformations and identify-

ing the operative mechanisms in specific cases may prove more difficult than detecting the

motion. Some of the potential contributors to postseismic deformation that have been suggested

include postseismic fault slip, viscoelastic relaxation of subsurface layers of the earth (Nur and

Mavko, 1974; Melosh, 1976; Rundle and Jackson, 1977, Thatcher and Rundle, 1979; Cohen,

1981a), fault creep at depth (Thatcher, 1974), flow of low viscosity magma regions (Wahr and

Wyss, 1980), and other forms of anelastic relaxation of surface and subsurface material (Cohen,

1980 a, b; Yang and Toksöz, 1981). Furthermore the pattern of deformation can be influenced

by horizontal and vertical variations in elastic (Mahrer and Nur, 1979) and anelastic material con-

stants, coseismic slip orientations (Mansinha and Smylie, 1971), and fault length, width, depth, etc.

The mechanism of crustal deformation of interest in this study is viscoelastic flow of sub-

crustal rocks. It is well established by experiments in rock mechanics that anelastic creep is a

function of rock type, temperature, stress, pressure and perhaps other parameters (Carter, 1976).

There is little doubt that there are conditions in the earth that can lead to some form of an-

elastic creep (Stocker and Ashby, 1973; Geotze and Evans, 1979); therefore it is not unreasonable

that viscoelastic responses have been invoked in studies of convection, postglacial rebound, earth

tidal deformation, seismic wave attenuation, and more recently postseismic rebound, The form

of the viscoelastic constitutive law is somewhat less certain. There are a number of laboratory

experiments for which non-linear flow laws of the form $\dot{\epsilon} = A\,\sigma^n\,f(P/T)$ where $\dot{\epsilon}$ is the deviatoric strain rate, σ is the deviatoric stress, f is a function of pressure, P, and temperature, T, and $n \simeq 3$ have been applied with success (Weertman and Weertman, 1975). It would not be surprising if a similar law is operative within some regions of the earth; however, the lack of knowledge of the earth's interior state, the existence of non-steady state stressing, and the existence of other geophysical complexities make the form of the rheological law or laws uncertain. In the present analysis I intend to use simpler linear viscoelastic rheologies in the development of models of postseismic deformation. The selection of a linear model is a simplification, but one which allows the separation of the coseismic and postseismic deformation and stress fields from preseismic ones. Although the model is conceptually clear, the mathematical and computational detail is sufficiently complex that a numerical, time-dependent finite element solution of the governing equations is justified.

MODEL DESCRIPTION

The model chosen for this study is shown in Figure 1, the rationale for the model has been discussed in Cohen (1981a). It is a multilayer model with a strike-slip fault embedded in the upper layer. The vertical strike-slip fault extends from an upper depth which may be zero (the surface of the earth), to a depth $\mathscr{D}$. The upper layer, the upper lithosphere, extends from the surface to a depth, H_1 (generally $H_1 \geq \mathscr{D}$ but there may be exceptions). This layer is characterized by the elastic parameter rigidity, μ_1. Below this layer to a depth H_2, lies the lower lithosphere represented by a standard viscoelastic solid with rigidities μ_{2a} and μ_{2b} and viscosity, η_2 as shown in the figure. Below the lithosphere, to a depth, H_3 lies the asthenosphere represented by a Maxwell viscoelastic fluid with rigidity, μ_3, and viscosity, η. Below the asthenosphere is an elastic mesosphere with rigidity, μ_4. The aforementioned rheological models represent the earth's deviatoric properties; the dilatational properties are assumed elastic throughout with associated bulk moduli k_1, k_2, k_3, and k_4. The choice of a standard linear solid lower lithosphere allows for an initial elastic response (rigidity, μ_a) to an applied constant strain, a partial stress relaxation

2

(on a time scale determined by η and the rigidities), and permanent support of a residual stress with a reduced rigidity, $\mu_a \mu_b / (\mu_a + \mu_b)$. Similarly, the Maxwell viscoelastic fluid model of the asthenosphere allows an initial elastic response (rigidity, μ_3) to an applied constant strain and subsequent stress relaxation (on a time scale controlled by η_3 and μ_3).

The mathematical description of the model can be developed by considering a substance that has standard linear solid deviatoric and elastic dilatational properties. This is the lower lithosphere element of the problem; other layers will be derived by evaluating various limiting forms of this general substance. The standard linear solid consists of a parallel combination of elastic and viscous elements (Kelvin element) in series with an elastic element. Although only the equations for the shear components of stress and strain, e.g. ϵ_{13} and ϵ_{23} will be needed in this analysis, the equations for all components will be derived as they will be needed for dip-slip analyses (Cohen, 1981b) and three dimensional calculations. For the elastic element of the Kelvin element the deviatoric constitutive relations are of the form

$$\frac{2\sigma_{11} - \sigma_{22} - \sigma_{33}}{3} = 2\mu_b \frac{(2\epsilon_{11} - \epsilon_{22} - \epsilon_{33})}{3} \tag{1a}$$

$$\sigma_{12} = 2\mu_b \epsilon_{12} \tag{1b}$$

where σ_{11} and ϵ_{11} are, for example, the $(1, 1)$ components of stress and strain respectively, and the quantities $(2\sigma_{11} - \sigma_{22} - \sigma_{33})/3$ and $(2\epsilon_{11} - \epsilon_{22} - \epsilon_{33})/3$ are the corresponding deviatoric stresses and strains of the normal components. For the viscous part of the Kelvin element the constitutive relations are

$$\frac{2\sigma_{11} - \sigma_{22} - \sigma_{33}}{3} = 2\eta \frac{d}{dt} \left[\frac{2\epsilon_{11} - \epsilon_{22} - \epsilon_{33}}{3} \right] \tag{2a}$$

$$\sigma_{12} = 2\eta \frac{d\epsilon_{12}}{dt} \tag{2b}$$

Since the Kelvin elements are connected in parallel the strains in equations 1 and 2 are equal and the stresses add; thus for the Kelvin element

$$2\sigma_{11} - \sigma_{22} - \sigma_{33} = 2\left(\mu_b + \eta\frac{d}{dt}\right)(2\epsilon_{11} - \epsilon_{22} - \epsilon_{33}) \tag{3a}$$

$$\sigma_{12} = 2\left(\mu_b + \eta\frac{d}{dt}\right)\epsilon_{12} \tag{3b}$$

or formally with $D = \dfrac{d}{dt}$

$$2\epsilon_{11} - \epsilon_{22} - \epsilon_{33} = \frac{1}{2(\mu_b + \eta D)}(2\sigma_{11} - \sigma_{22} - \sigma_{33}) \tag{4a}$$

$$\epsilon_{12} = \frac{1}{2(\mu_b + \eta D)}\sigma_{12} \tag{4b}$$

In analogy with equation 1, for the elastic element in series with the Kelvin substance,

$$2\epsilon_{11} - \epsilon_{22} - \epsilon_{33} = \frac{2\sigma_{11} - \sigma_{22} - \sigma_{33}}{2\mu_a} \tag{5a}$$

$$\epsilon_{12} = \frac{\sigma_{12}}{2\mu_a} \tag{5b}$$

The series elements have equal stresses and their strains add, hence for the combined three element standard linear solid

$$2\epsilon_{11} - \epsilon_{22} - \epsilon_{33} = \frac{1}{2}\left[\frac{1}{\mu_a} + \frac{1}{\mu_b + \eta D}\right]\left[2\sigma_{11} - \sigma_{22} - \sigma_{33}\right] \tag{6a}$$

$$\epsilon_{12} = \frac{1}{2}\left[\frac{1}{\mu_a} + \frac{1}{\mu_b + \eta D}\right]\sigma_{12} \tag{6b}$$

or rearranging

$$2\dot{\sigma}_{11} - \dot{\sigma}_{22} - \dot{\sigma}_{33} + \frac{(\mu_a + \mu_b)}{\eta}(2\sigma_{11} - \sigma_{22} - \sigma_{33}) =$$

$$2\mu_a(2\dot{\epsilon}_{11} - \dot{\epsilon}_{22} - \dot{\epsilon}_{33}) + \frac{2\mu_a \mu_b}{\eta}(2\dot{\epsilon}_{11} - \dot{\epsilon}_{22} - \dot{\epsilon}_{33}) \tag{7a}$$

$$\dot{\sigma}_{12} + \frac{(\mu_a + \mu_b)}{\eta}\sigma_{12} = 2\mu_a \dot{\epsilon}_{12} + \frac{2\mu_a \mu_b}{\eta}\epsilon_{12} \tag{7b}$$

where the dots above the symbols indicate time derivatives.

4

The next step is to impose the condition that the dilatation is elastic

$$\sigma_{11} + \sigma_{22} + \sigma_{33} = 3k(\epsilon_{11} + \epsilon_{22} + \epsilon_{33}) \tag{8}$$

Solving equation 8 for $\sigma_{22} + \sigma_{33}$ and inserting in equation 7a results in

$$\dot{\sigma}_{11} + \frac{(\mu_a + \mu_b)}{\eta} \sigma_{11} = \left[\frac{3k + 4\mu_a}{3}\right] \dot{\epsilon}_{11} + \left[\frac{3k - 2\mu_a}{3}\right] (\dot{\epsilon}_{22} + \dot{\epsilon}_{33}) +$$

$$\left[\frac{3k + 4\dfrac{\mu_a \mu_b}{\mu_a + \mu_b}}{3}\right] \frac{(\mu_a + \mu_b)}{\eta} \epsilon_{11} + \left[\frac{3k - 2\dfrac{\mu_a \mu_b}{\mu_a + \mu_b}}{3}\right] \frac{(\mu_a + \mu_b)}{\eta} (\epsilon_{22} + \epsilon_{33}) \tag{9}$$

Writing $\mu = \mu_a$, $\mu' = \dfrac{\mu_a \mu_b}{\mu_a + \mu_b}$ and $\tau = \eta/(\mu_a + \mu_b)$ the general equations are

$$\dot{\sigma}_{11} + \frac{\sigma_{11}}{\tau} = \left(\frac{3k + 4\mu}{3}\right) \dot{\epsilon}_{11} + \left(\frac{3k - 2\mu}{3}\right) (\dot{\epsilon}_{22} + \dot{\epsilon}_{33}) + \left(\frac{3k + 4\mu'}{3}\right) \frac{\epsilon_{11}}{\tau} +$$

$$\left(\frac{3k - 2\mu'}{3}\right) \left(\frac{\epsilon_{22} + \epsilon_{33}}{\tau}\right) \tag{10a}$$

$$\dot{\sigma}_{22} + \frac{\sigma_{22}}{\tau} = \left(\frac{3k + 4\mu}{3}\right) \dot{\epsilon}_{22} + \left(\frac{3k - 2\mu}{3}\right) (\dot{\epsilon}_{11} + \dot{\epsilon}_{22}) + \left(\frac{3k + 4\mu'}{3}\right) \frac{\epsilon_{22}}{\tau} +$$

$$\left(\frac{3k - 2\mu'}{3}\right) \left(\frac{\epsilon_{11} + \epsilon_{33}}{\tau}\right) \tag{10b}$$

$$\dot{\sigma}_{33} + \frac{\sigma_{33}}{\tau} = \left(\frac{3k + 4\mu}{3}\right) \dot{\epsilon}_{33} + \left(\frac{3k - 2\mu}{3}\right) (\dot{\epsilon}_{11} + \dot{\epsilon}_{22}) + \left(\frac{3k + 4\mu'}{3}\right) \frac{\epsilon_{33}}{\tau} +$$

$$\left(\frac{3k - 2\mu'}{3}\right) \left(\frac{\epsilon_{11} + \epsilon_{22}}{\tau}\right) \tag{10c}$$

$$\dot{\sigma}_{12} + \frac{\sigma_{12}}{\tau} = 2\mu\dot{\epsilon}_{12} + \frac{2\mu'}{\tau} \epsilon_{12} \tag{10d}$$

$$\dot{\sigma}_{13} + \frac{\sigma_{13}}{\tau} = 2\mu\dot{\epsilon}_{13} + \frac{2\mu'}{\tau} \epsilon_{13} \tag{10e}$$

$$\dot{\sigma}_{23} + \frac{\sigma_{23}}{\tau} = 2\mu\dot{\epsilon}_{23} + \frac{2\mu'}{\tau} \epsilon_{23} \tag{10f}$$

5

Equations 10 form a system of equations with standard linear solid deviatoric and elastic dilatational properties. A system with Maxwell deviatoric properties can be derived by letting $\mu_b \to 0$. This implies $\mu' \to 0$ and, for example

$$\dot{\sigma}_{11} = \left(\frac{3k + 4\mu}{3}\right)\dot{\epsilon}_{11} + \left(\frac{3k - 2\mu}{3}\right)(\dot{\epsilon}_{22} + \dot{\epsilon}_{33}) - \frac{1}{\tau}[\sigma_{11} - k(\epsilon_{11} + \epsilon_{22} + \epsilon_{33})] \qquad (11a)$$

$$\dot{\sigma}_{12} + \frac{\sigma_{12}}{\tau} = 2\mu\dot{\epsilon}_{12} \qquad (11b)$$

A purely elastic substance can be derived from equation 11 by letting $\tau \to \infty$, then

$$\sigma_{11} = \left(\frac{3k + 4\mu}{3}\right)\epsilon_{11} + \left(\frac{3k - 2\mu}{3}\right)(\epsilon_{22} + \epsilon_{33}) \qquad (12a)$$

$$\sigma_{12} = 2\mu\epsilon_{12} \qquad (12b)$$

In the finite element analysis I have used a two dimensional grid in which the directions are depth and distance from the fault. The displacements (for a strike slip fault) are orthogonal to this plane in the direction of the 3 axis). The technique for solving equations 10 in the finite element analysis is presented in Appendix A.

Having derived the rheological equations, and implemented the finite element technique for solving them, the next step for computing the quasi-static displacement, strains, and stresses is to define the input numerical parameters of the model. The parameters that affect the model calculations are the fault slip, the depths of top and bottom boundaries of the fault slip zone, the layer boundaries H_1, H_2, and H_3 and the elastic and viscous parameters of the layers. For simplicity I have chosen to set equal all the rigidities with $\mu_1 = \mu_{2a} = \mu_{2b} = \mu_3 = \mu_4 = 5 \times 10^{11}$ dyne/cm^2 and bulk moduli with $k_1 = k_2 = k_3 = k_4 = 8.33 \times 10^{11}$ dyne/cm^2. These values correspond to Young's moduli of 1.25×10^{12} dyne/cm^2, and Poisson's ratio of 0.25. The viscosity of the lower lithosphere is chosen to be 1×10^{21} poise and that of the presumably warmer asthenosphere 5×10^{19} poise. The associated time constants for stress relaxation are $\tau_2 = \eta_2/(\mu_{2a} + $

μ_{2b}) $= 1 \times 10^9$ sec $\simeq 32$ yrs., and $\tau_3 = \eta_3/\mu_3 = 1 \times 10^8$ sec ≈ 3 yrs. Frequently in succeeding paragraphs I will examine results at five particular times:

$$t_o = 0^+ \text{ sec}$$

$$t_a = 1 \cdot 10^8 \text{ sec} = \tau_3 = 0.1 \, \tau_2 \approx 3 \text{ yrs}$$

$$t_b = 5 \cdot 10^8 \text{ sec} = 5\tau_3 = 0.5 \, \tau_2 \approx 16 \text{ yrs}$$

$$t_c = 1 \cdot 10^9 \text{ sec} = 10\tau_3 = \tau_2 \approx 32 \text{ yrs}$$

$$t_d = 5 \cdot 10^9 \text{ sec} = 50\tau_3 = 5\tau_2 \approx 159 \text{ yrs}$$

The slip function is set equal to 1 meter from the top of the fault (the surface of the earth in the present calculations) to a depth D; then by way of continuity of displacement within the finite elements displacement decreases linearly toward 0 at the node below D (generally 10 km lower). The slip enters the calculations as a scale constant; thus, the reported values of displacements, strains, and stresses are normalized per one meter slip. The bottom of the computational grid is arbitrarily selected at 800km, the ends of the grid at ±4000km sufficiently far from the source region that the boundary conditions (free or fixed) do not affect the results. The remaining parameters of the model are D, and H_1, the depth of the boundary between the upper and lower lithosphere, H_2, the depth of the lower lithosphere–asthenosphere boundary and H_3, the depth of the asthenosphere–mesosphere boundary. I designate model calculations by the notation (D), H_1, H_2, H_3 where the numerical values are given in kilometers.

RESULTS

The starting point for presenting the results of model calculations will be model (20), 30, 75, 400 for which the coseismic slip plane terminates at the top of the lower lithosphere at a depth of thirty kilometers. The calculated displacements are shown as a function of distance from the fault and time following the earthquake in Figure 2. Appreciable postseismic displacements extend over a broad zone extending to several hundred kilometers from the fault. The peak displacement is about 7 cm at time $t_b \approx 16$ yrs. and about 15 cm at time $t_d \approx 159$ yrs. There are considerable similarities in the displacement versus distance curves at various times,

however, the location of the peak displacement does vary somewhat. This peak point, which is a transition point from positive to negative postseismic strain, ϵ_{13}, is at $X \simeq 150$km at time $t_a \simeq$ 3 yrs. and at $X \simeq 200$km at $t_d \simeq 159$ yrs. The details of the time dependent motion of the peak will be discussed below.

It is instructive as to the development of the postseismic deformation to examine the subsurface displacement and stress fields. Figure 3 shows the coseismic displacements at three depths: the surface of the earth, the bottom of the slip region, (i.e. the top of the lower lithosphere), and top of the asthenosphere. The gradient of these curves gives the coseismic strain, ϵ_{13}, (in all the numerical results presented herein engineering strains are used) or to within a multiplicative constant, the initial stress, σ_{13}, acting in a plane parallel to the fault. The curves show the initial stress drop (negative gradient) at the surface of the earth and significant stress rises (positive gradients) near the fault below the slip region. In response to the applied stresses the viscoelastic regions begin to flow. The flow produces a time dependent stress relaxation as shown in Figure 4a. The asthenosphere, which has a shorter relaxation time than the lower lithosphere, accomplishes about 90% of its complete, near fault, relaxation of the coseismic stress of 0.51×10^6 dyne/cm^2 within about 5×10^8 sec. $\simeq 16$ yrs. The more sluggish lower lithosphere responds over a long time scale and of course maintains a residual permanent stress field. There is significant restressing of the surface that accompanies the subsurface relaxation and flow. The time dependent surface and subsurface strain changes accompanying these stress changes are shown in Figure 4b. The detailed dependence of the surface stress and strain on distance from the fault and time is shown in Figure 5. Although the postseismic strains are commonly smaller in magnitude than the coseismic ones, they are more broadly distributed. For example at time, t_d, the postseismic stress is reduced by one-half from its peak value over a distance of about 35 km; by contrast the coseismic strain drops by one-half over 20 km. The broad zone of postseismic deformation is, of course, a reflection of the deep position of the flowing viscoelastic layers.

Another way of studying the spatial and temporal dependence of the stress (or deformation) fields is to plot contours of constant postseismic stress on a distance-time grid as shown in Figure 6a. This sketch illustrates that the region of positive postseismic stress advances from within ~135 km at $t = 1 \times 10^8$ sec to ~189 km at $t = 5 \times 10^9$ sec. Other contours of constant stress show similar progressions away from the fault with time. Figure 6b shows the corresponding contours of constant stress when the lithosphere is modeled as an elastic substance rather than as elastic layer over a viscoelastic one. Particularly noteworthy in Figure 6b is the greater extent of the positive postseismic stress zone, noticeably at long times. The damped advancement of the postseismic stress field in the case of the layered viscoelastic profile can be understood by considering the depths and response times of the layers. First as the asthenosphere relaxes it induces surface displacements which are zero at the fault, rise to a peak, then decrease further away. As relaxation progresses the peak moves further from the fault implying an advancement of the zone of postseismic restressing. As the lower lithosphere begins to relax, however, it too produces surface displacements, ones that will be relatively near the fault. Thus the advance of the displacement peak away from the fault with time will be retarded and the zone of positive restressing narrowed, but the magnitudes of the near fault stress recovery will be increased. This point is emphasized in Figure 7 which shows the rate of horizontal displacement versus distance and time. A comparison of Figure 7a for the viscoelastic lower lithosphere model and Figure 7b for the elastic lower lithosphere models shows that in the former case and at long times there is a broader zone of significant displacement rates.

The coseismic and postseismic displacements vary not only with distance from the fault, but also with depth from the surface. This gives use to the stress and strain components, σ_{23}, and ϵ_{23} respectively. Whereas σ_{13} acts on a plane parallel to the fault, σ_{23} acts on a plane parallel to the earth's surface. As Figure 8 illustrates ϵ_{23} is generally less than σ_{13} at most points near the surface but becomes of greater relative significance at depth. The corresponding depth, distance, and time dependent strains are shown in Figure 9.

9

As illustrated earlier it is instructive to compare the present calculations of surface deformations with those which ignore viscoelasticity in the lower lithosphere by considering an elastic lithosphere over a viscoelastic asthenosphere. Figure 10 shows a comparison of the calculated displacements versus distance and time. The curves are similar in shape in the two models but differ significantly in magnitude, most noticeably at long time when relaxation of the upper lithosphere has had sufficient opportunity to occur; at $t = t_d$, the maximum difference in the curves is about 6 cm at $X = 75$ km. Of perhaps greater significance is the difference in strains. Figure 11 shows the ratio of the modeled strains versus distance and time. Near the fault the effect of creep in the lower lithosphere is to produce a three-fold increase in the postseismic restraining over a time of 159 years.

Another aspect of the calculation that bears investigation is the effect of changes in the layer depths on surface displacements. Figure 12a, for example, shows the effect of changing the depth of the lower lithosphere-asthenosphere boundary, H_2, after a time $t_b \approx 16$ yrs. Of particular note is the fact that the position of the peak of the postseismic displacement pattern is fairly sensitive to the depth of the top of the asthenosphere. The closer H_2 is to the bottom of the slip region the greater the initial stressing of the asthenosphere and the greater the subsequent postseismic deformation. The sensitivity of the deformation pattern to H_2 suggests that observations of postseismic displacements may be useful for determining the depth to the top of the asthenosphere (if such observations can be sufficiently stripped of other contaminating signals from, e.g., plate motion). By contrast the location of the bottom of the asthenosphere is not well resolved by the shape of the displacement curve or by the amplitude (Figure 12b). Similarly the shape of the displacement vs. distance curve at time t_d is not very sensitive to the depth of the top of the creeping lower lithosphere (Figure 12c) although, the displacements are enhanced as the distance between the creep zone and the slip area is reduced. The sensitivity of the displacement curve shape to H_1 is increased only slightly when the displacements at time t_b are subtracted from those at t_d to estimate the long time scale component of displacement. The effect of reducing

fault lower depth on coseismic and postseismic displacements are shown in Figure 13. Both the coseismic and postseismic displacements are larger for the more deeply extending fault. However, while the coseismic strain drop is reduced, the near-fault postseismic strain recovery is increased by increasing D.

CONCLUSIONS

The viscoelastic rebound effects discussed in this paper will be significant when the depths of the anelastic relaxation layers are not much greater than the bottom of the fault slip zone. There is insufficient data currently available to decide whether such a situation exists on any major strike-slip fault of the earth. Predicted peak postseismic strains of 10–100 μstrains following major earthquakes are, however, detectable by surveying techniques, although measurement interpretation may be ambiguous. The model calculations presented here have shown that the spatial and temporal patterns of postseismic deformation can be sensitive to the depth of the creep region and the viscosity structure of the earth, however, the spatial-temporal pattern is less sensitive to creep region thickness. It is possible that definitive models of the deformation of the earth during the earthquake cycle will require attention to multilayer viscoelastic effects as well as other factors such as lateral and vertical variations in slip, rheological properties, rock type, etc.

ACKNOWLEDGEMENTS

APPENDIX

Melosh and Raefsky (1980) have discussed the use of the explicit algorithm of Cormeau (1975) and the implicit algorithm of Hughes and Taylor (1978) for finite element analyses of equations of the form

$$\dot{\sigma} = D(\dot{\epsilon} - \dot{\epsilon}^{vp}) \tag{A1}$$

where D is the matrix of elastic parameters and $\dot{\epsilon}^{vp}$ is a function of stress. The explicit algorithm cited above is also applicable when $\dot{\epsilon}^{vp}$ is a function of strain as well as stress, and the reader is referred to these papers for a description of the technique. In this appendix equations 10 of the text are recast in the form of equation A1 so the algorithm can be applied. Specifically applying equation A1 to the normal components of $\dot{\sigma}$ in equation 10 results in

$$
\begin{bmatrix}
\dfrac{3k+4\mu}{3} & \dfrac{3k-2\mu}{3} & \dfrac{3k-2\mu}{3} \\[2ex]
\dfrac{3k-2\mu}{3} & \dfrac{3k+4\mu}{3} & \dfrac{3k-2\mu}{3} \\[2ex]
\dfrac{3k-2\mu}{3} & \dfrac{3k-2\mu}{3} & \dfrac{3k+4\mu}{3}
\end{bmatrix}
\begin{bmatrix}
\dot{\epsilon}_{11}^{vp} \\[2ex]
\dot{\epsilon}_{21}^{vp} \\[2ex]
\dot{\epsilon}_{33}^{vp}
\end{bmatrix}
= \frac{\mu+\mu_b}{\eta}
\begin{bmatrix}
\sigma_{11} \\[2ex]
\sigma_{21} \\[2ex]
\sigma_{33}
\end{bmatrix}
-
$$

$$
\frac{\mu+\mu_b}{\eta}
\begin{bmatrix}
\dfrac{3k+4\mu'}{3} & \dfrac{3k-2\mu'}{3} & \dfrac{3k-2\mu'}{3} \\[2ex]
\dfrac{3k-2\mu'}{3} & \dfrac{3k+4\mu'}{3} & \dfrac{3k-2\mu'}{3} \\[2ex]
\dfrac{3k-2\mu'}{3} & \dfrac{3k-2\mu'}{3} & \dfrac{3k+4\mu'}{3}
\end{bmatrix}
\begin{bmatrix}
\epsilon_{11} \\[2ex]
\epsilon_{22} \\[2ex]
\epsilon_{33}
\end{bmatrix}
\tag{A2}
$$

from which

$$\begin{bmatrix} \dot{e}_{11}{}^{vp} \\ \dot{e}_{22}{}^{vp} \\ \dot{e}_{33}{}^{vp} \end{bmatrix} = \frac{\mu + \mu_b}{18\eta k\mu} \begin{bmatrix} 2(3k+\mu) & -(3k-2\mu) & -(3k-2\mu) \\ -(3k-2\mu) & 2(3k+\mu) & -(3k-2\mu) \\ -2(3k-2\mu) & -2(3k-2\mu) & 2(3k+\mu) \end{bmatrix} \begin{bmatrix} \sigma_{11} \\ \sigma_{22} \\ \sigma_{33} \end{bmatrix}$$

$$- \frac{1}{3\eta} \begin{bmatrix} \mu + 3\mu_b & \mu & \mu \\ \mu & \mu + 3\mu_b & \mu \\ \mu & \mu & \mu + 3\mu_b \end{bmatrix} \begin{bmatrix} \epsilon_{11} \\ \epsilon_{22} \\ \epsilon_{33} \end{bmatrix} \qquad (A3)$$

It is convenient to eliminate σ_{33} through equation 8. Then

$$\begin{bmatrix} \dot{e}_{11}{}^{vp} \\ \dot{e}_{22}{}^{vp} \\ \dot{e}_{33}{}^{vp} \end{bmatrix} = \frac{\mu + \mu_b}{2\eta\mu} \begin{bmatrix} 1 & 0 \\ 0 & 1 \\ -1 & -1 \end{bmatrix} \begin{bmatrix} \sigma_{11} \\ \sigma_{22} \end{bmatrix} -$$

$$\frac{1}{3\eta\mu} \begin{bmatrix} \dfrac{3k(\mu+\mu_b)+4\mu\mu_b}{2} & \dfrac{3k(\mu+\mu_b)-2\mu\mu_b}{2} & \dfrac{3k(\mu+\mu_b)-2\mu\mu_b}{2} \\[2mm] \dfrac{3k(\mu+\mu_b)-2\mu\mu_b}{2} & \dfrac{3k(\mu+\mu_b)+4\mu\mu_b}{2} & \dfrac{3k(\mu+\mu_b)-2\mu\mu_b}{2} \\[2mm] -3k(\mu+\mu_b)-\mu\mu_b & -3k(\mu+\mu_b)-\mu\mu_b & -3k(\mu+\mu_b)+2\mu\mu_b \end{bmatrix} \begin{bmatrix} \epsilon_{11} \\ \epsilon_{22} \\ \epsilon_{33} \end{bmatrix} \qquad (A4)$$

The shear equation corresponding to A4 is simply

$$\begin{bmatrix} \dot{e}_{12}{}^{vp} \\ \dot{e}_{13}{}^{vp} \\ \dot{e}_{23}{}^{vp} \end{bmatrix} = \frac{\mu + \mu_b}{2\mu\eta} \begin{bmatrix} \sigma_{12} \\ \sigma_{13} \\ \sigma_{23} \end{bmatrix} - \left(\frac{\mu + \mu_b}{\eta}\right)\frac{\mu'}{\mu} \begin{bmatrix} \epsilon_{12} \\ \epsilon_{13} \\ \epsilon_{23} \end{bmatrix} \qquad (A5)$$

For the problem studied in this paper only the (1, 3) and (2, 3) components of the stress and strain need be considered. For the dip-slip problem the (1, 1), (2, 2), and (1, 2) components are relevant (Cohen, 1981b).

13

REFERENCES

Brown, L. D., R. E. Reilinger, S. R. Holdahl, and E. J. Balazs, "Postseismic Crustal Uplift Near Anchorage Alaska," J. Geophys. Res., 82, 3369–3378, 1977.

Carter, N. L., "Steady State Flow of Rocks," Rev. Geophys. Space Phys., 14, 301–360, 1976.

Cohen, S. C., "Postseismic Viscoelastic Surface Deformation and Stress, 1, Theoretical Considerations, Displacement, and Strain Calculations," J. Geophys. Res., 85, 3131–3150, 1980a.

Cohen, S. C., "Postseismic Viscoelastic Surface Deformation and Stress, 2, Stress Theory and Computation, Dependence of Displacement, Strain, and Stress on Fault Parameters," J. Geophys. Res., 85, 3151–3158, 1980b.

Cohen, S. C., "Postseismic Rebound Due to Creep of the Lower Lithosphere and Asthenosphere," Geophys. Res. Letters, 8, 493–496, 1981a.

Cohen, S. C., "Postseismic Rebound Due to Creep of the Lower Lithosphere and Asthenosphere," EOS Trans. Am. Geophys. Union, 62, 401, 1981b.

Cormeau, I. C., "Numerical Stability in Quasi-static Elasto/visco-plasticity," Int. J. Numer. Meth. Engrg., 9, 109-127, 1975.

Dunbar, W. S., D. M. Boore, and W. Thatcher, "Pre-, Co-, and Post-seismic Strain Change Associated with the 1952 M_L = 7.2 Kern County, California, Earthquake, Bull. Seismol. Soc. Am., 70, 1893–1905, 1980.

Geotze, C., and B. Evans, "Stress and Temperature in the Bending Lithosphere as Constrained by Experimental Rock Mechanics," Geophys. J. Roy. Astron. Soc., 59, 463–478, 1979.

Hughes, T. J. P., and P. L. Taylor, "Unconditionally Stable Algorithms for Quasi-static Elasto/Visco-plastic Finite Element Analysis," Comput. Struct., 8, 169-175, 1978.

Mahrer, K. D., and A. Nur, "Static Strike–Slip Faulting in a Horizontally Varying Crust," Bull. Seismol. Soc. Am., 69, 975–1009, 1979.

Mansinha, L., and D. E. Smylie, "The Displacement Fields of Inclined Faults," Bull. Seismol. Soc. Am., 61, 1433–1440, 1971.

Melosh, H. J., "Nonlinear Stress Propagation in the Earth's Upper Mantle," J. Geophys. Res., 81, 5621–5632, 1976.

Melosh, H. J., and A. Raefsky, "The Dynamical Origin of Subduction Zone Topography," Geophys. J. Roy. Astron. Soc., 60, 333–354, 1980.

Nur, A., and G. Mavko, "Postseismic Viscoelastic Rebound," Science, 183, 204–206, 1974.

Rundle, J. B., and D. D. Jackson, "A Three–Dimensional Viscoelastic Model of a Strike–Slip Fault," Geophys. J. Roy. Astron. Soc., 49, 565–591, 1977.

Stocker, R. L., and M. F. Ashby, "On the Rheology of the Upper Mantle," Rev. Geophys. Space Phys., 11, 391–426, 1973.

Thatcher, W., "Strain Release Mechanism of the 1906 San Francisco Earthquake," Science, 1984, 1283–1285, 1974.

Thatcher, W., "Strain Accumulation and Release Mechanism of the 1906 San Francisco Earthquake," J. Geophys. Res., 80, 4862–4872, 1975.

Thatcher, W., T. Matsuda, T. Kato, and J. B. Rundle, "Lithospheric Loading by the 1896 Riku-u Earthquake, Northern Japan: Implications for Plate Flexure and Asthenosphere Rheology," J. Geophys. Res., 85, 6429–6435, 1980.

Thatcher, W., and J. B. Rundle, "A Model for the Earthquake Cycle in Underthrust Zones," J. Geophys. Res., 84, 5540–5556, 1979.

Wahr, J., and M. Wyss, "Interpretation of Postseismic Deformation with a Viscoelastic Relaxation Model," J. Geophys. Res., 85, 6471–6477, 1980.

Weertman, J., and J. R. Weertman, "High Temperature Creep of Rock and Mantle Viscosity," Ann. Rev. Earth Plan. Sci., 3, 293–315, 1975.

Yang, M., and M. N. Toksöz, "Time–Dependent Deformation and Stress Relaxation After Strike Slip Earthquakes," J. Geophys. Res., 86, 2889–2901, 1981.
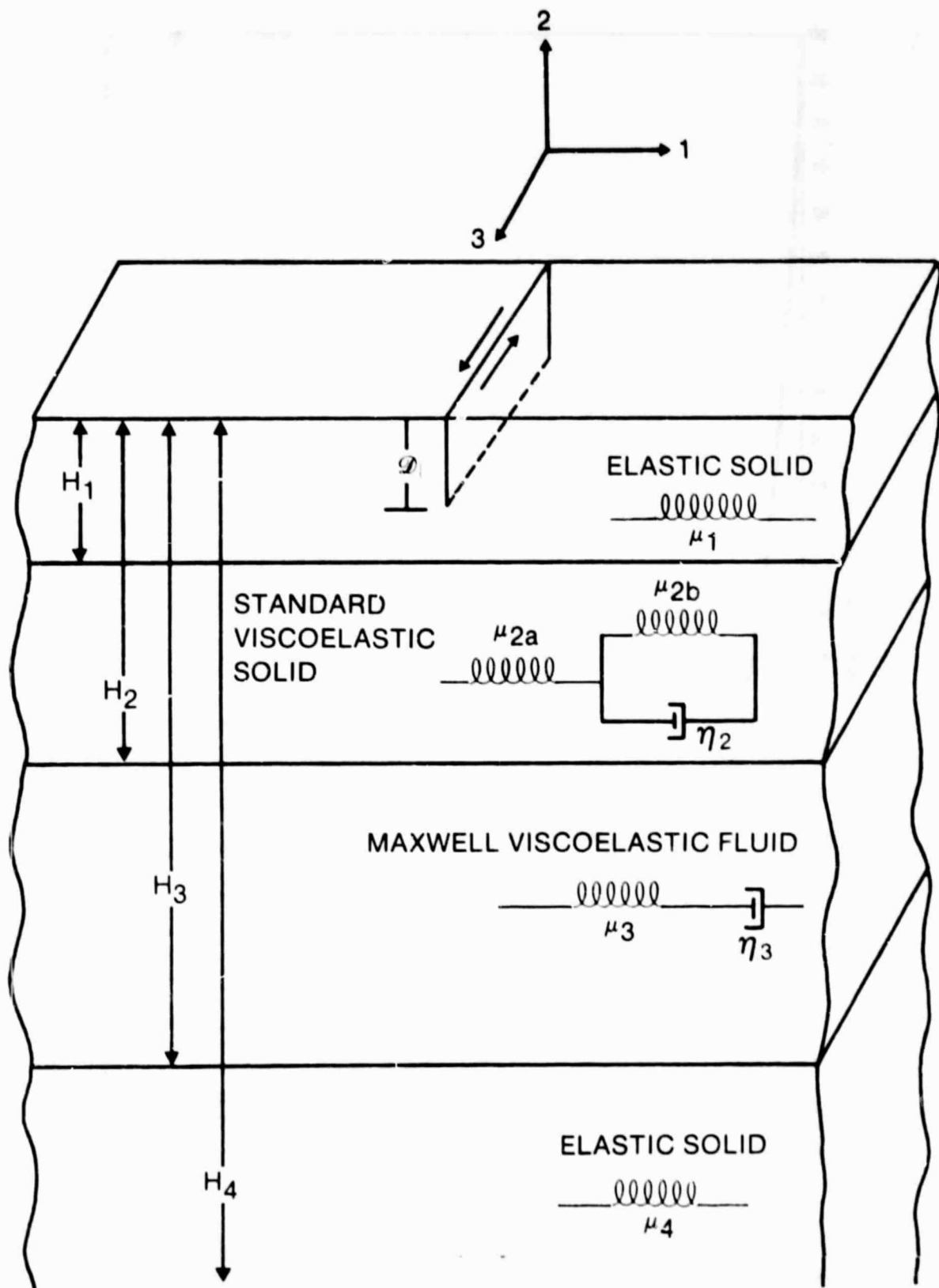
FIGURE CAPTIONS

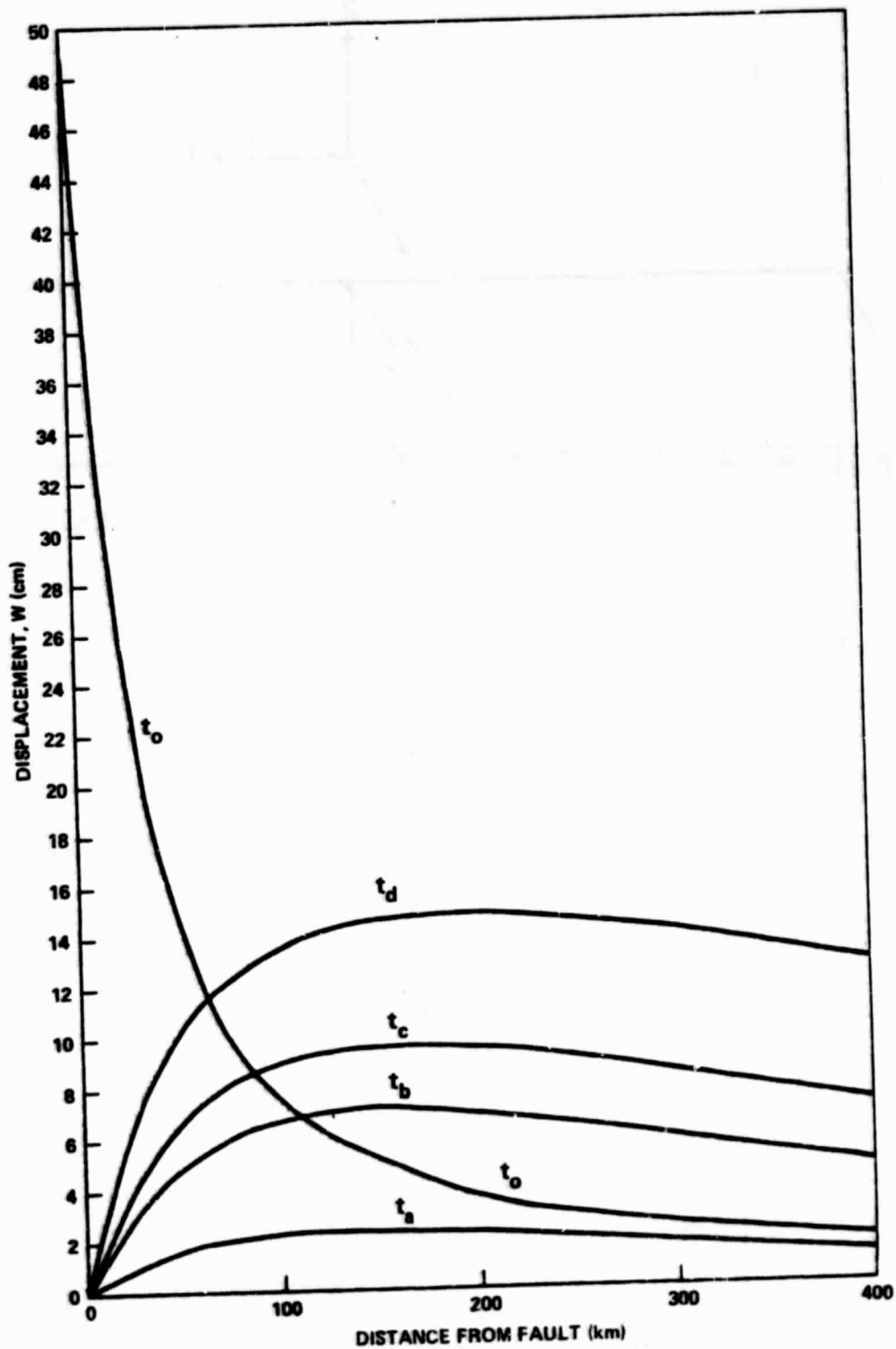Figure 1.   Multilayer rheological model for postseismic rebound study.

Figure 2.   Displacement versus distance; coseismic displacement at time t_o; postseismic displacements ($\Delta W = W(t) - W(t_o)$) at times $t_a = 1 \cdot 10^8$ sec $\approx$ 3 yrs, $t_b = 5 \cdot 10^8$ sec $\approx$ 16 yrs, $t_c = 1 \cdot 10^9$ sec $\approx$ 31 yrs, $t_d = 5 \cdot 10^9$ sec $\approx$ 159 yrs.
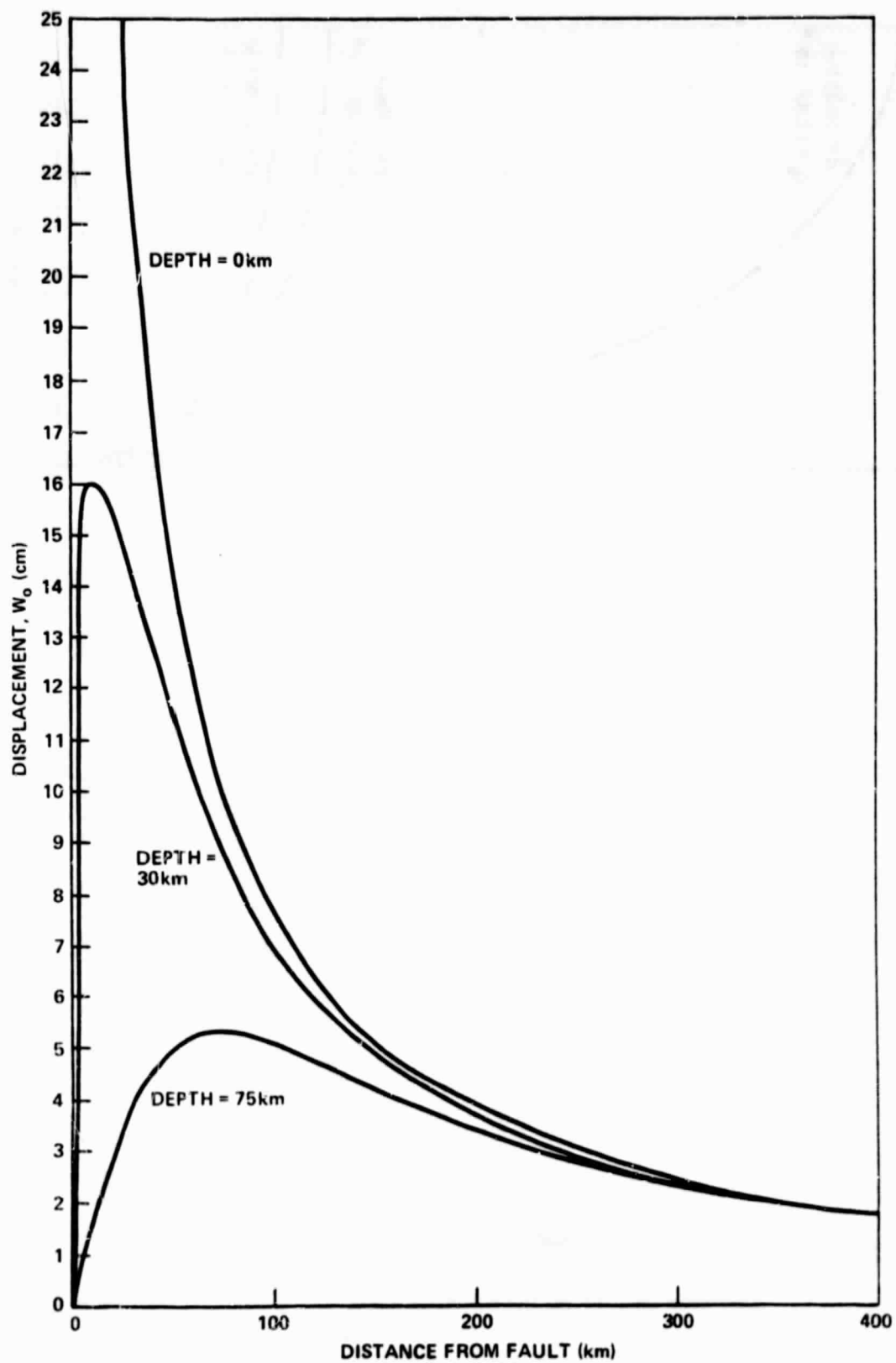
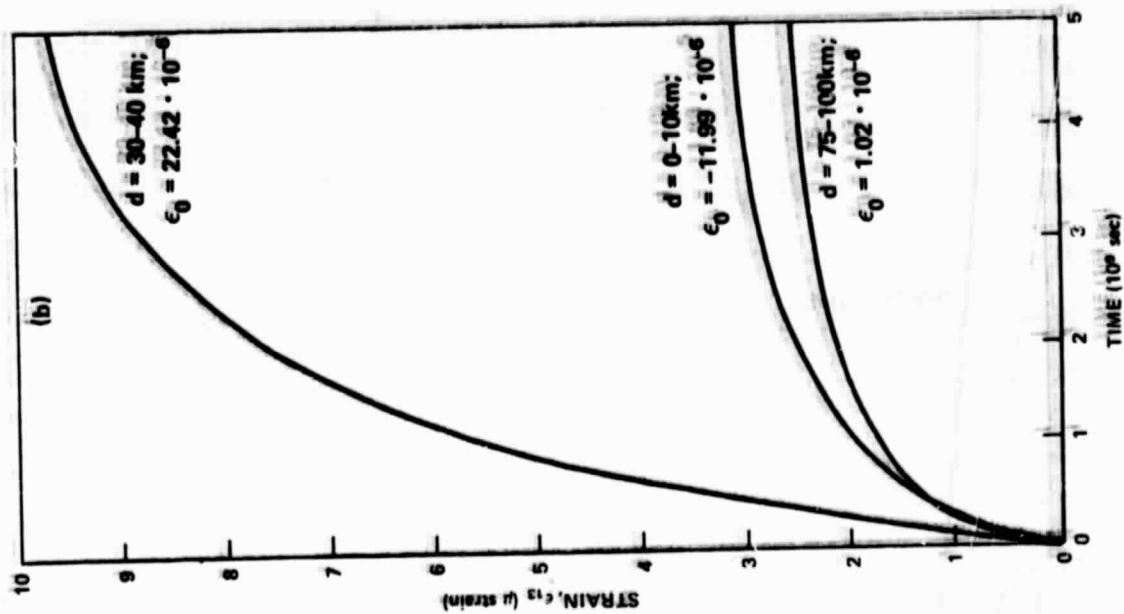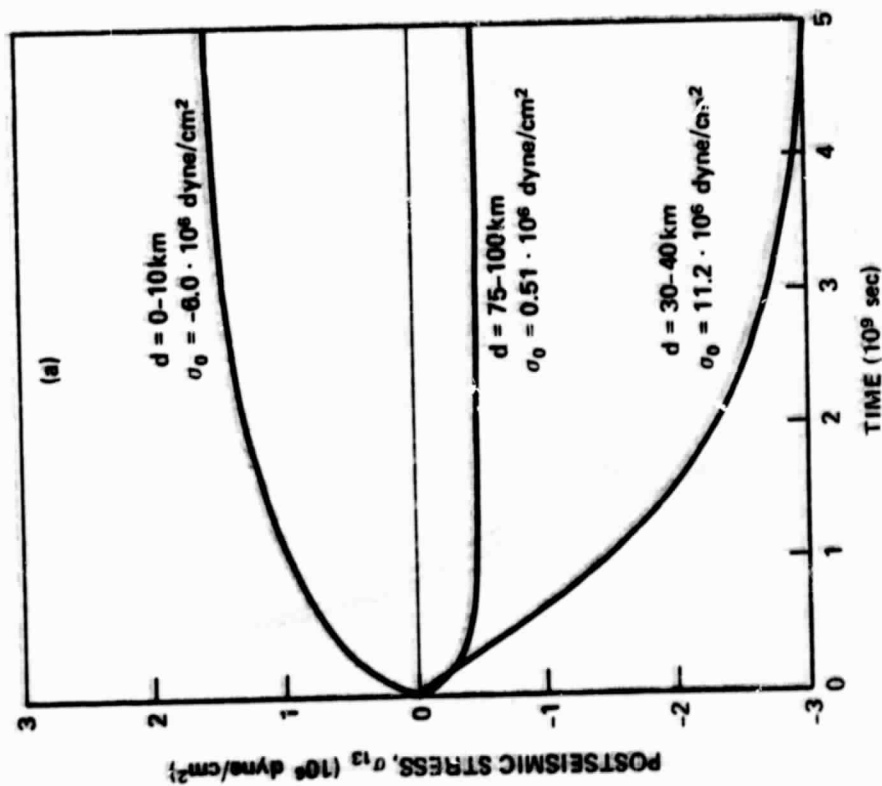Figure 3.   Coseismic displacements versus distance at various depths.

Figure 4a.   Near-fault stress versus time at various depths. Stress is averaged over a grid element extending from 1–10km from the fault and over indicated depth ranges.

Figure 4b.   Near-fault strain versus time at various depths.

Figure 5.   Stress (strain) versus distance from fault at various depths.

Figure 6.   Contours of constant postseismic stress (units of 10^6 dyne/cm^2) on a distance from fault–time after earthquake grid. a. Model (20), 30, 75, 400 with viscoelastic lower lithosphere. b. Model (20), 75, 75, 400 with elastic lower lithosphere.

Figure 7.   Rate of horizontal displacement versus distance from fault at various times. a. Model (20), 30, 75, 400. b. Model (20), 75, 75, 400.

Figure 8.   Stress components, σ_{13} and σ_{23}, versus distance from fault at various times and depths. a. Depth = 0–10km, b. depth = 30–40km, c. depth = 75–100km, (note vertical scale change for c).

Figure 9.   Strain components, ϵ_{13} and ϵ_{23}, versus distance from fault at various times and depths. a. Depth = 0–10km, b. depth = 30–40km, c. depth = 75–100km.

Figure 10.   Comparisons of postseismic displacement patterns at various times for models with and without a viscoelastic lower lithosphere.

Figure 11. Ratio of near surface postseismic strain for viscoelastic lower lithosphere to near sur-
face postseismic strain for elastic lower lithosphere as a function of distance from
the fault and time.

Figure 12. Postseismic surface displacement versus distance from fault for various layer interface
depths and selected times. a. Lower lithosphere – asthenosphere boundary, H_2, varied,
$t = t_b$, b. asthenosphere – mesosphere boundary, H_3, varied, $t = t_b$, c. upper litho-
sphere – lower lithosphere boundary, H_1, varied, $t = t_d$.

Figure 13. Coseismic and postseismic displacements versus distance from fault for different
width faults. Solid lines model (20), 30, 75, 400, dashed lines model (10), 30, 75,
400.

Figure 1. Multilayer rheological model for postseismic rebound study.

Figure 2. Displacement versus distance; coseismic displacement at time t_o; postseismic displacements ($\Delta W = W(t) - W(t_o)$) at times $t_a = 1 \cdot 10^8$ sec ≈ 3 yrs, $t_b = 5 \cdot 10^8$ sec ≈ 16 yrs, $t_c = 1 \cdot 10^9$ sec ≈ 31 yrs, $t_d = 5 \cdot 10^9$ sec ≈ 159 yrs.

18

Figure 3. Coseismic displacements versus distance at various depths.

Figure 4b. Near-fault strain versus time at various depths.

Figure 4a. Near-fault stress versus time at various depths. Stress is averaged over a grid element extending from 1-10km from the fault and over indicated depth ranges.

20

Figure 5. Strain (stress) versus distance from fault at various depths.

21

Figure 6. Contours of constant postseismic stress (units of 10^6 dyne/cm^2) on a distance from fault–time after earthquake grid, a. model (20), 30, 75, 400 with viscoelastic lower lithosphere, b. model (20), 75, 75, 400 with elastic lower lithosphere.

22

Figure 7. Rate of horizontal displacement versus distance from fault at various times, a. model (20), 30, 75, 400, b. model (20), 75, 75, 400.

23

Figure 8. Stress components, σ_{13} and σ_{23}, versus distance from fault at various times and depths, a. depth = 0-10km, b. depth = 30-40km, c. depth = 75-100km, (note vertical scale change for c).
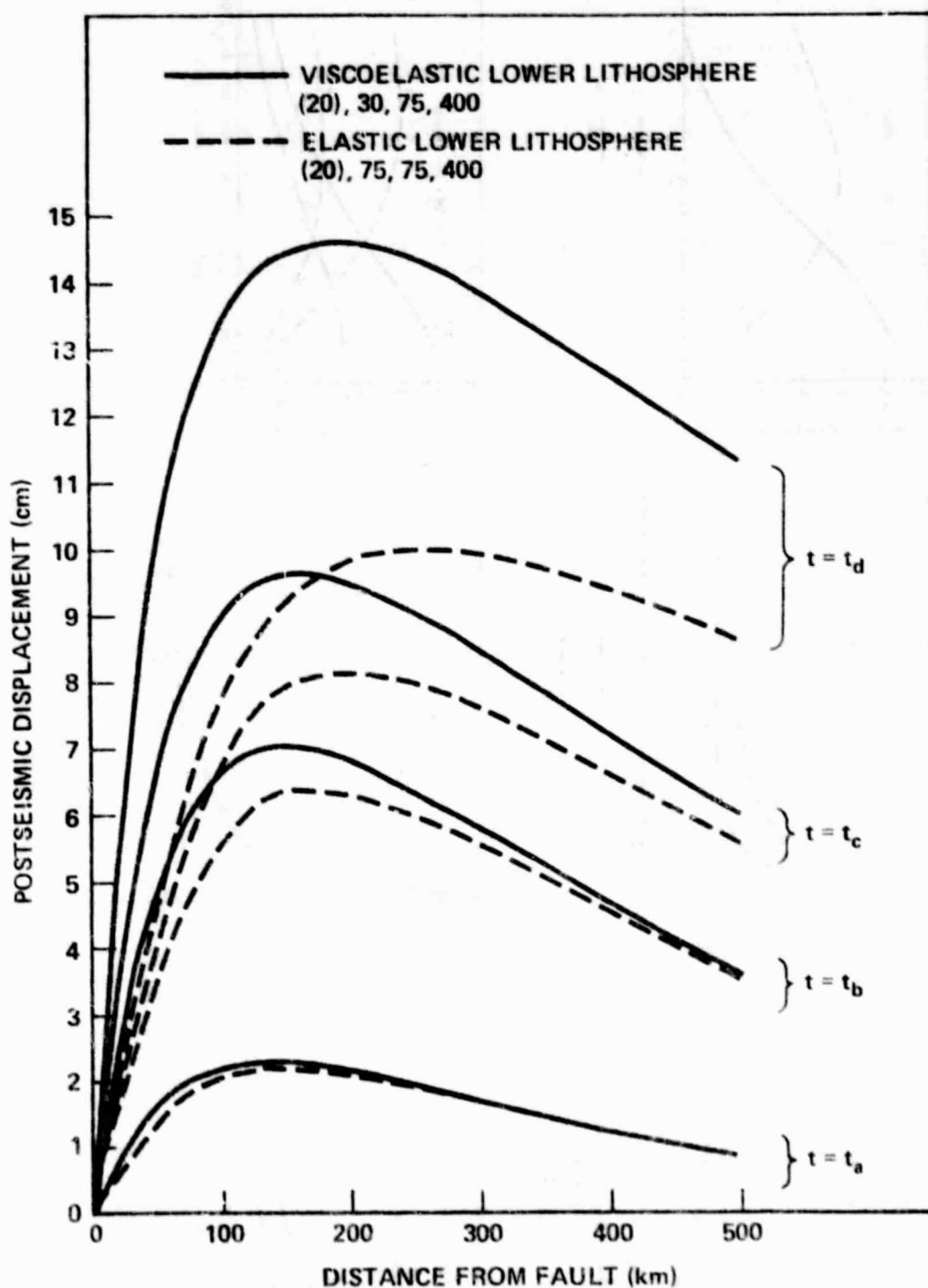
24

Figure 9. Strain components ϵ_{13} and ϵ_{23}, versus distance from fault at various times and depths. a. depth = 0–10km. b. depth = 30–40km. c. depth = 75–100km.

Figure 10. Comparisons of postseismic displacement patterns at various times for models with and without a viscoelastic lower lithosphere.
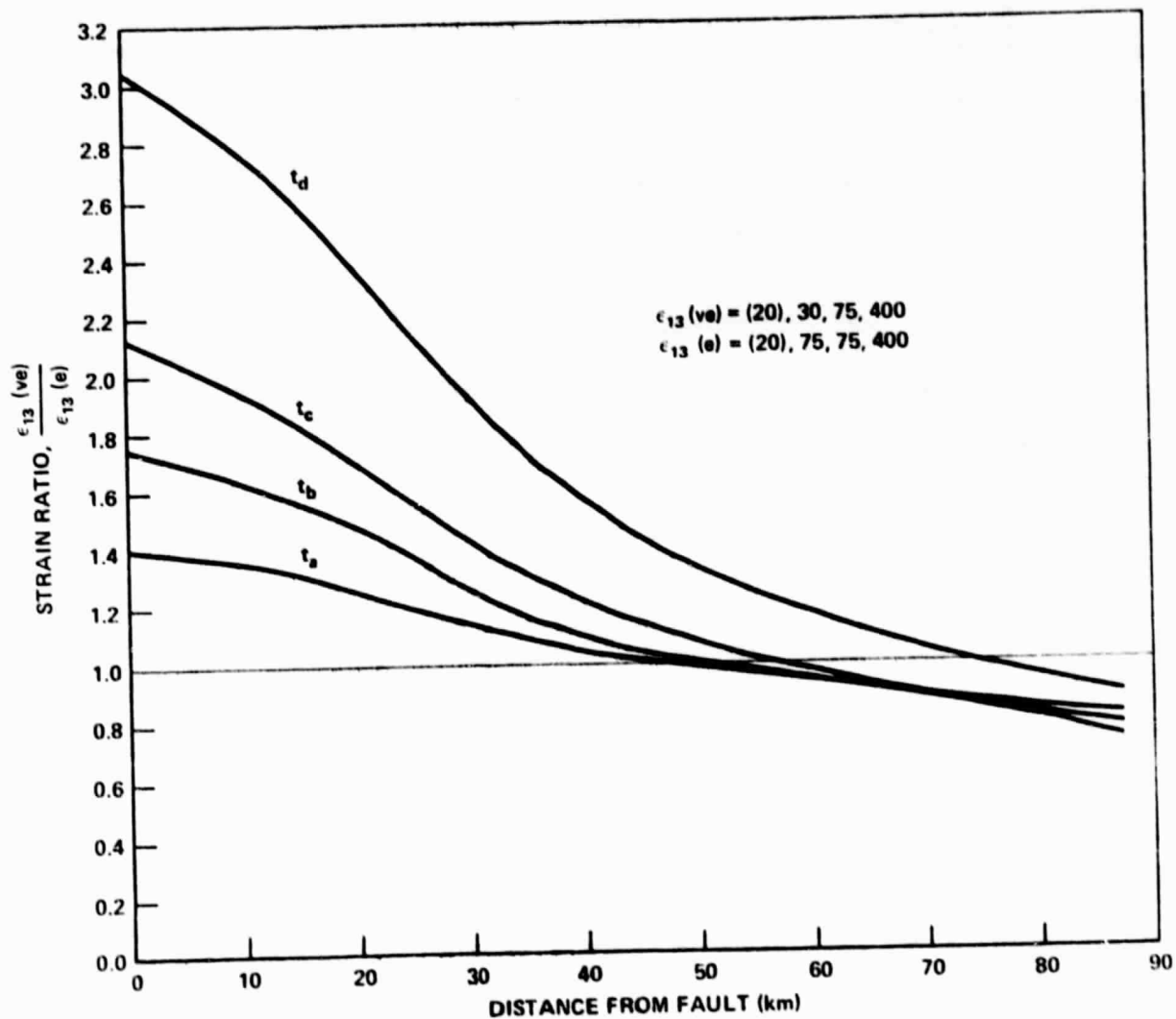
Figure 11. Ratio of near surface postseismic strain for viscoelastic lower lithosphere to near surface postseismic strain for elastic lower lithosphere as a function of distance from the fault and time.
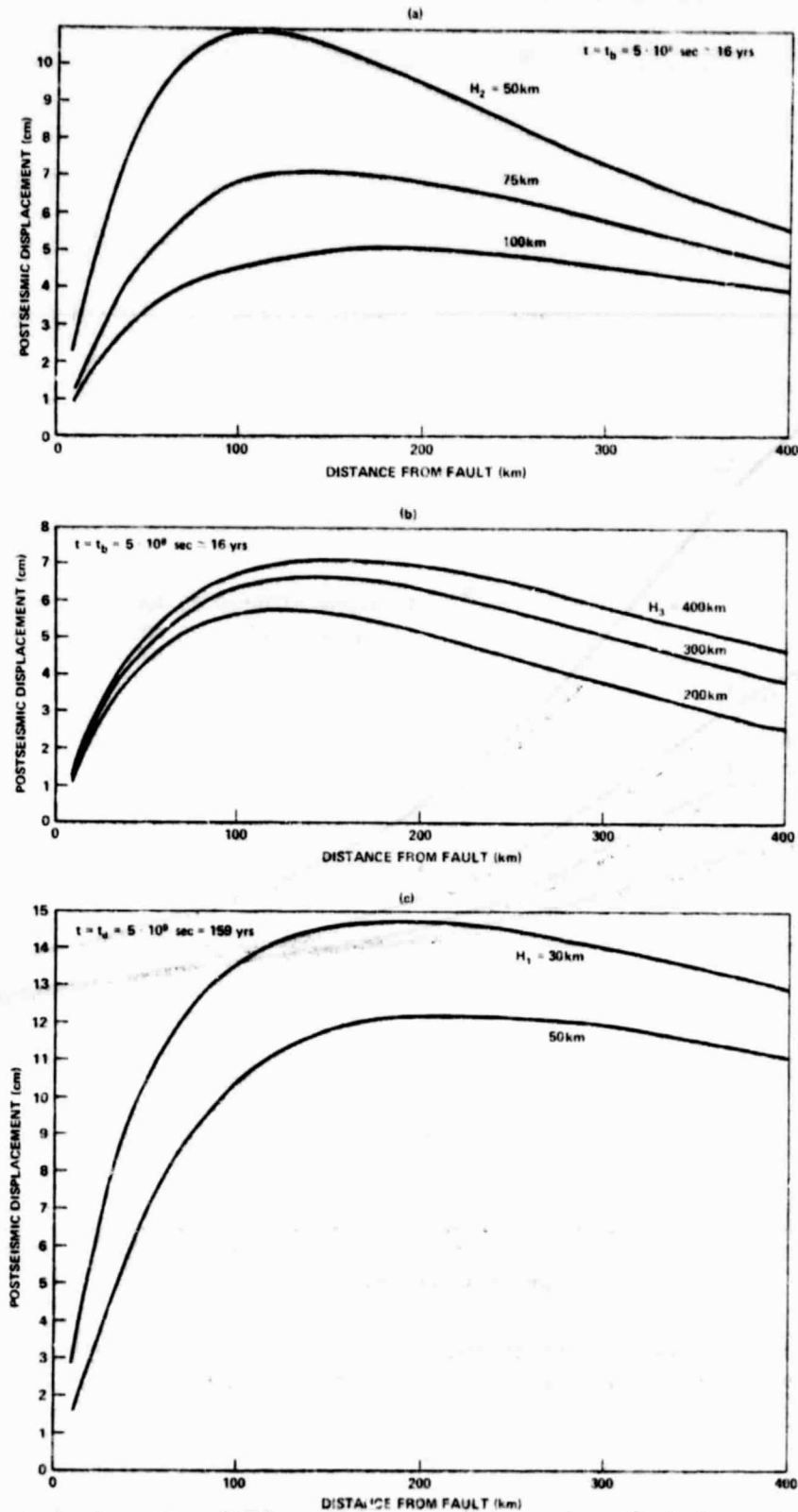
Figure 12. Postseismic surface displacement versus distance from fault for various layer inter-face depths and selected times, a. lower lithosphere – asthenosphere boundary, H_2, varied, $t = t_b$, b. asthenosphere – mesosphere boundary, H_3, varied, $t = t_b$, c. upper lithosphere – lower litho-sphere boundary, H_1, varied, $t = t_d$.
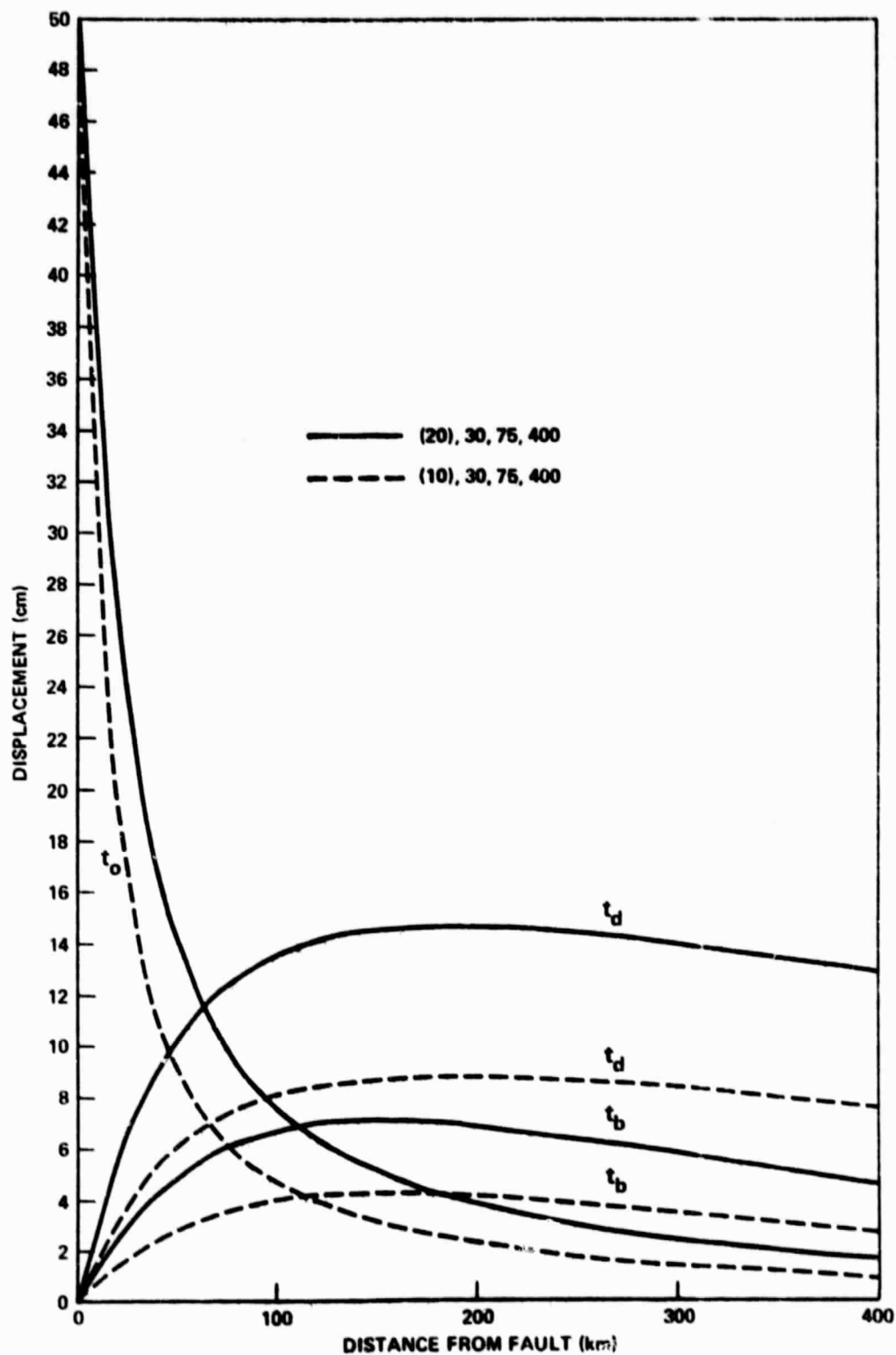
Figure 13. Coseismic and postseismic displacements versus distance from fault for different width faults. Solid lines model (20), 30, 75, 400, dashed lines model (10), 30, 75, 400.